NUMERICAL SIMULATION OF UNSTEADY ROTATIONAL FLOW OVER PROPFAN CONFIGURATIONS

NASA GRANT No. NAG-3-730

SEMI-ANNUAL STATUS REPORT

For the Period

May 1, 1989 - November 30, 1989

Submitted to

NASA LEWIS RESEARCH CENTER
CLEVELAND, OHIO

Attn: George Stefko
Chief, Structural Dynamics Branch

Prepared By

R. Srivastava
Graduate Research Assistant

L. N. Sankar
Associate Professor

School of Aerospace Engineering
Georgia Institute of Technology
Atlanta, GA 30332

November 1989

INTRODUCTION

The objective of this research is to develop efficient numerical techniques for the study of aeroelastic response of a propfan in an unsteady transonic flow. A three dimensional unsteady Euler solver, developed at Georgia Institute of

The subject report is forwarded in conformance with the contract/grant specifications.

Should you have any questions or comments reguarding this report, please contact the Project Director or the undersigned.

Sincerely.

Mary M. Wolfe
Research Reports Coordinator

ws

Distribution:
Addressee, 3 copies
NASA Sci & Tech Info Fac., 2 copies

AN EQUAL EDUCATION AND EMPLOYMENT OPPORTUNITY INSTITUTION

, 1989

ınd propfan
ər numerical
f the solver
dy the effect
solver were
lations were

flexibility on
lted in large
ıat for future
for.

ənted in the
əno, Nevada
ɔf the text of

)-APRIL

ɔlve counter
ultation with
ing propeller

APPENDIX

Application of an Efficient Hybrid Scheme for Aeroelastic Analysis of Advanced Propellers

by

R. Srivastava* and N. L. Sankar**
Georgia Institute of Technology
Atlanta, GA

and

T. S. R. Reddy† and D. L. Huff††
NASA Lewis Research Center
Cleveland, OH

* Graduate Student, Member AIAA and AHS
** Associate Professor, Member AIAA and AHS
† Resident Research Associate, Member AIAA and AHS
†† Research Engineer, Member AIAA

Application of an Efficient Hybrid Scheme for Aeroelastic Analysis of Advanced Propellers

Abstract

An efficient three dimensional hybrid scheme is applied for solving Euler equations to analyze advanced propellers. The scheme treats the spanwise direction semi explicitly and the other two directions implicitly, without affecting the accuracy, as compared to a fully implicit scheme. This leads to a reduction in computer time and memory requirement.

The calculated power coefficients for two advanced propellers, SR3 and SR7L, and various advance ratios showed good correlation with experiment. Spanwise distribution of elemental power coefficient and steady pressure coefficient differences also showed good agreement with experiment. A study of the effect of structural felxibility on the performance of the advanced propellers showed that structural deformation due to centrifugal and aero loading should be included for better correlation.

Introduction

It has been known for some time now that the best propulsive efficiency is offered by propellers. However the efficiency drops off very rapidly as the cruise Mach number increases beyond 0.5, as high tip Mach numbers lead to high compressibility losses (due to wave drag). Currently an effort is underway to improve the propulsive efficiency of commercial and military aircraft. Newly designed high speed advanced propellers, also known as propfans, show a very high propulsive efficiency at cruise speeds upto Mach 0.8 [1].

The propfans are designed to delay the compressibility losses, thus extending the high efficiency of a propeller to relatively higher cruise Mach numbers. This is accomplished by sweeping the blade backwards and using thinner airfoils, on

improved on this method by using the curved lifting line concept to account for the sweep. In this approach the vortex wake is represented by a finite number of vortex filaments in place of the continuous sheet of vorticity as used in Goldstein's approach. The analysis has been further extended in reference [5] by placing the vortex filaments along the stream surfaces so that they conform to the shape of the axisymmetric nacelle.

Hanson [6] and Williams [7] applied the Kernel function approach to a propfan blade. They numerically solve a linear integral equation for upwash angle due to the blade pressure distribution by discretizing the load representation. The friction drag is obtained from the two- dimensional airfoil tables as a function of lift coefficient for the appropriate section camber, thickness and a Mach number adjusted for sweep and three-dimensional effects. The induced drag is obtained by determining the kinetic energy-per-unit-length of the far wake. The methods mentioned so far are based on linearized analyses. However, as the advanced propeller operates at or near transonic tip Mach number, flow nonlinearties may become important.

Jou [8] has applied the finite volume approach of Jameson [9] for the analysis of propfans using full potential equation. The formulation was not able to provide converged solutions for free stream Mach numbers greater than 0.6. It was concluded that strong rotational flow effects were present near the leading edge, which could not be modelled by the potential equation. In addition the potential flow equations at times, lead to non-unique solutions.

Chausee [10] and Whitfield *et al.* [11] have applied the unsteady, three dimensional Euler equations to the propfan geometry. Matsuo *et al.* [12] have recently solved the full Navier - Stokes equations around a propfan. Some of these methods have been reviewed in reference [13], with regards to performance prediction.

All the analyses mentioned so far, with the exception of Whitfield *et al.* [11] have been for axisymmetric flows. For a propfan in flight configuration, the flow is not axisymmetric. Even for cruise conditions the nacelle is at an angle of attack

explicitly requires only two costly inversions of block tridiagonal matrix, as opposed to three inversions for a fully implicit scheme, per time step. It also reduces the memory requirement as only two time levels of information needs to be stored at any given time, one of which needs to be only two dimensional. The use of such a hybrid scheme leading to reduction in computer time and memory requirement, makes the scheme more efficient.

The specific objectives of the present paper are 1) to apply an efficient hybrid scheme to analyze advanced propellers, 2) to calculate steady performance, 3) to include structural deformation, due to centrifugal and steady aero loading in the analysis, 4) to study the effects of structural flexibility on the performance of advanced propellers. The governing equations and the numerical solution method are described first followed by results and discussion. The methods developed here are expected to be helpful for future aeroelastic research.

Formulation

Aerodynamic Model:

The Euler equations, in conservation form, in Cartesian coordinate system can be written as:

$$(\hat{\mathbf{q}})_t + (\hat{\mathbf{E}})_x + (\hat{\mathbf{F}})_y + (\hat{\mathbf{G}})_z = 0 \tag{1}$$

where $\hat{\mathbf{q}}$ is the vector containing conserved flow properties. $\hat{\mathbf{E}}, \hat{\mathbf{F}}$ and $\hat{\mathbf{G}}$ are the nonlinear flux vectors which are functions of the vector $\hat{\mathbf{q}}$. The subscripts denote the partial derivative of the vector. In the above equation

$$\begin{aligned} \xi &= \xi(x,y,z,t) \\ \eta &= \eta(x,y,z,t) \\ \zeta &= \zeta(x,y,z,t) \\ \tau &= t \end{aligned} \tag{4}$$

These coordinates are non orthogonal and completely general. The equation (1) can be rewritten as:

$$\mathbf{q}_\tau + \mathbf{E}_\xi + \mathbf{F}_\eta + \mathbf{G}_\zeta = 0 \tag{5}$$

where

$$\mathbf{q} = J^{-1}\begin{pmatrix} \rho \\ \rho u \\ \rho v \\ \rho w \\ e \end{pmatrix} \qquad \mathbf{E} = J^{-1}\begin{pmatrix} \rho U \\ \rho u U + \xi_x p \\ \rho v U + \xi_y p \\ \rho w U + \xi_z p \\ (e+p)U - \xi_t p \end{pmatrix}$$

$$\mathbf{F} = J^{-1}\begin{pmatrix} \rho V \\ \rho u V + \eta_x p \\ \rho v V + \eta_y p \\ \rho w V + \eta_z p \\ (e+p)V - \eta_t p \end{pmatrix} \qquad \mathbf{G} = J^{-1}\begin{pmatrix} \rho W \\ \rho u W + \zeta_x p \\ \rho v W + \zeta_y p \\ \rho w W + \zeta_z p \\ (e+p)W - \zeta_t p \end{pmatrix} \tag{6}$$

U, V, and W are the contravariant velocities, and J is the jacobian and ξ_x, η_x, ζ_x etc. are the metrics of transformation.

Initial and Boundary Conditions

A large number of problems can be described by the same set of governing

inflow boundary, all quantities are fixed to that of the free stream,as disturbances cannot travel upstream in a supersonic flow. At the subsonic outflow boundary, four characteristics should escape, thus the four quantities $\rho, \rho u, \rho v, \rho w$ are extrapolated from inside while the pressure is fixed to that of the free stream. For supersonic outflow, all characteristics should escape, hence all quantities are extrapolated from inside the flow domain.

The block interface boundary :

It is neither efficient nor practical to solve all the blades at the same time, hence, one blade passage is handled at a time. This introduces additional boundaries for computation. Across these boundaries all the variables must be continuous, except on solid boundaries and boundaries downstream of the blade. The boundary condition, for these boundaries, depends on the type of flow being solved. An axisymmetric flow would require periodicity on the fluid interface boundaries. Periodicity will require that the two boundaries have same fluid properties. As shown in figure (1a), the fluid properties at the boundaries K=1 and K=KMAX are updated as the average of fluid properties at K=2 and K=KMAX-1 for a symmetric flow field.

For an unsymmetric flow, the periodicity on these boundaries does not exist. Therefore, in order to obtain the solution for such a case, the whole propfan should be solved. This is done by advancing the solution of each block one time step, one block at a time. In this case again the boundaries are updated explicitly, after the interior points have been updated.This is done by averaging the flow variables from the nodes on each side of the boundary from the adjoining blocks. Referring to figure (1b), (the subscripts refer to the corresponding block) the quantities at boundary K=KMAX of block N (which is also the boundary K=1 for block N+1) would be the average of flow quantities at K=KMAX-1 of block N and K=2 of block

marching direction is reversed after every sweep, in order to remove any dependency on the marching direction. Equation (10) can then be rewritten as :

$$\mathbf{q}^{n+1} = \mathbf{q}^n - \Delta\tau \left(\mathbf{E}_\xi^{n+1} + \mathbf{F}_\eta^{n,n+1} + \mathbf{G}_\zeta^{n+1} \right) \tag{11}$$

Since the η marching direction is changed every iteration, the $\mathbf{F}_\eta^{n,n+1}$ alternates between

$$\frac{\mathbf{F}^n_{i,j+1,k} - \mathbf{F}^{n+1}_{i,j-1,k}}{2\Delta\eta}$$

during the odd time steps, and

$$\frac{\mathbf{F}^{n+1}_{i,j+1,k} - \mathbf{F}^n_{i,j-1,k}}{2\Delta\eta}$$

during the even time steps.

The above discretization leads to a set of algebraic equations for $\mathbf{q}$. These equations are costly to solve since the flux vectors $\mathbf{E}$ and $\mathbf{G}$ are highly nonlinear. The nonlinearity is removed by linearising the fluxes about the previous time step value, resulting in the following linear equation :

$$\left[I + \Delta\tau \left(\delta_\xi A^n + \delta_\zeta B^n \right) \right] \mathbf{q}^{n+1} = \left[I + \Delta\tau \left(\delta_\xi A^n + \delta_\zeta B^n \right) \right] \mathbf{q}^n + \mathbf{R}^{n,n+1} \tag{12}$$

where

$$\mathbf{R}^{n,n+1} = -\Delta\tau \left(\delta_\xi \mathbf{E}^n + \delta_\eta \mathbf{F}^{n,n+1} + \delta_\zeta \mathbf{G}^n \right) \tag{13}$$

and the operator notation $\delta_\xi(A\mathbf{q}) = [\delta_\xi A]\mathbf{q}$ and $\delta_\zeta(B\mathbf{q}) = [\delta_\zeta B]\mathbf{q}$ is used.

This Euler equation formulation can be very easily extended to solve the Navier-Stokes equations by simply adding the viscous terms to the right hand side. This does not alter the numerical formulation.

name 'Alternating Direction'. These inversions are performed at each spanwise station, marching along the spanwise direction. As mentioned earlier, the marching direction is reversed every iteration. Each element of the block tridiagonal matrix has 5×5 elements.

Artificial Dissipation:

The use of central difference, makes the scheme mildly unstable, and also introduces odd even decoupling. This is remedied by adding artificial dissipation. The implementation of artificial dissipation, in the present work is based on the formulation of Jameson et al. [16]. This scheme has a second order implicit dissipation and a blend of second/ fourth difference explicit dissipation terms. A scaling factor for both implicit and explicit dissipation is employed to control the amount of dissipation in the scheme. Adding the dissipation terms, equations (18) and (19) can be written as:

$$\left[I + \Delta\tau\left(\delta_\xi A^n + \epsilon_I D_{I_\xi}\right)\right]\Delta\mathbf{q}^{*n+1} = \mathbf{R}^{n,n+1} - \epsilon_E D_E \Delta\tau \qquad (20)$$

$$\left[I + \Delta\tau\left(\delta_\zeta B^n + \epsilon_I D_{I_\zeta}\right)\right]\Delta\mathbf{q}^{n+1} = \Delta\mathbf{q}^{*n+1} \qquad (21)$$

where D_{I_ξ} and D_{I_ζ} are second order implicit dissipation terms and D_E is the explicit dissipation term, given in reference [22]. ϵ_I and ϵ_E are user supplied constants, which depend on grid spacing. At the boundaries the fourth order differences are repalced by second order differences.

Aeroelastic Model:

As mentioned earlier, the propfan has thin, swept, and twisted blades. Since the blades are thin and flexible, deflections due to centrifugal and steady aero loads are large. Hence, the aeroelastic problem is inherently nonlinear, requiring geometric nonlinear theory of elasticity [17].

The blades have large sweep and twist, which couples blade bending and tor-

i.e., until the change in deflection from the $(i+1)^{th}$ iteration is equal to that from the i^{th} iteration.

Results and Discussion

The hybrid numerical scheme discussed in the previous section, was first applied to an isolated aircraft wing in reference [21] and to a helicopter rotor blade in reference [22]. Typical results showing blade loading, are reproduced in figures (3) and (4). As can be seen from both these figures, the hybrid scheme is able to predict flow phenomena of varying complexity with fairly good degree of accuracy.

The propfan blade has a much more complex shape than the aircraft wing or the helicopter blade. The high twist, large sweep, low aspect ratio, close proximity of other blades, presence of nacelle and thinner blades near the tip, make the flow field around it very complex. In the following, the flow solutions obtained for two advanced propellers, namely SR3 and SR7L, are presented. The calculations have been performed on a 'hot shape', obtained by including the deflections due to centrifugal loading in the undeflected blade shape ('cold shape').

A body fitted H-O grid was used for these calculations. A typical grid used in the calculation is shown in figure (5). The domain of calculation was taken to be the region between two blades with upper surface of one blade and lower surface of the adjoining blade as the boundaries of the domain. This region is referred to as blade passage. In general, in order to model the influence of adjacent blades (cascade effect) the entire propfan with all the blades (passages) are solved. However, for an axisymmetric flow field, considered here, all blade passages can be assumed to be identical, and only one blade passage is solved enforcing the conditions of symmetry.

SR3 Propfan

The hybrid scheme, described earlier, was used to solve the flow field around an 8-bladed SR3 propfan. The SR3 propfan was designed to operate at a free stream Mach number of 0.8, advance ratio of of 3.06, at an altitude of 30,000 feet.

an overprediction in the tip region results in an under prediction on the inboard region.

SR7L Propfan

The SR7L propfan has been designed for an operating free stream Mach number of 0.8, rotational speed of 1700 rpm, at an altitude of 35,000 feet. In this section calculations for a two bladed SR7L propfan are presented. The aerodynamic calculations are first performed on the 'hot shape'. The effect of blade flexibility is then included in the calculations.

In figure (8) the elemental pressure coefficient difference is compared with experiment for a 2-bladed SR7L propfan. The blade was operating at a free stream Mach number of 0.775 and advance ratio of 3.088. The 75% span setting angle was adjusted to match the power coefficient by a rigid body rotation of the blade about the pitch change axis. The pressure coefficient difference ΔC_p $(C_{p_l} - C_{p_u})$ is plotted and compared against experimental data [27] at various span locations. The comparison is good, except near the leading edge on the outboard stations.

The effect of blade flexibility on performance was studied next for the SR7L propfan blade. The effect of flexibility is included by the aeroelastic iteration process, described earlier and shown in figure (2).

It is important that the blade finite element model accurately reflects its structural characteristics, since the entire analysis process is centered around the stiffness matrix. The NASTRAN finite element model used in this study is based on the final blade design [24]. The SR7L blade has an aluminum spar, nickel sheath, and fiber glass shell with foam fill. The shell, adhesive, spar, and shell filler material were combined using the Composite Blade Structural Analysis (COBSTRAN) program to produce equivalent, monolithic shell elements [25]. The finite element model of the SR7L blade is shown in figure (9a). The model has 261 nodes and 449 triangular shell elements. Bar elements are used to model the shank. Multipoint constraint grid chords are used to define the shank/blade interface [26].

the final blade shape.

In figure (11) the thrust coefficient is plotted against the power coefficient for subsequent iterations. The setting angle used in the calculations has been obtained by rigid body rotation of the hot shape so as to match the power coefficient obtained by experiments. The experimental point is also plotted. The power coefficient obtained from the hot shape (marked 1), compares well with the experiment. However, the power coefficient changes considerably (marked 2 to 4), as the blade is allowed to deform under this load. It can be seen from figures (10) and (11), that the initial change in shape, lead to large change in power coefficient. For this particular case, under which the blades are loaded heavily almost 40% change in power coefficient is observed when the effect of aerodynamic loading is included in the blade shape. The subsequent changes are not as large. Hence, in order to obtain a better comparison with experimental power coefficient and load distribution on blade, the blade setting angle should be chosen such that the converged shape power coefficient is compared against the experimental data. This requires some trial and error in selecting the 'cold' or 'hot' shape from which the aeroelastic iteration should be started. Arriving at the final blade shape might be critical for vibration and flutter calculations, as well.

In figure(12) the relative change in twist angle over the span is plotted. This shows that the largest deflection occurs near the tip, with practically no deflection on the root sections. Also it should be noted that the variation in the blade twist is nonlinear and is largest near the tip. A rigid body rotation of the blade to account for the change in twist, would result in a linear variation along the span. This clearly shows that for better performance calculations, structural flexibility should be included in the analysis.

Figure (13) shows the in-plane deflection of the blade planform and figure (14) shows the out of plane deflection of the blade at constant chord. Again, the largest deflection is towards the tip, with practically no deflection towards the root. Figure

4. The effect of aero loads was to compensate for the untwisting due to centrifugal loads

Acknowledgements

The authors wish to acknowledge Dr. Richard August of Sverdrup Technology Inc., Cleveland, OH, for many helpful suggestions. This work has been carried out under NASA grant NAG3-730 from NASA Lewis Research Center in Cleveland, Ohio, Mr. George L. Stefko, grant monitor.

References

[1] Whitlow, J. B., Jr. and Sievers, G. K.," Fuel Savings Potential of the NASA ATP," NASA TM 83736, 1984.

[2] Mehmed, O. and Kaza, K. R. V., " Experimental Classical Flutter Results of a Composite Advanced Turboprop Model," NASA TM-88792

[3] Goldstein, S.," On the Vortex Theory of Screw Propellers," Royal Society Proceedings, Vol. 123, No. 792, Apr. 6, 1929, pp 440-465

[4] Sullivan, J. P.," The effect of Blade Sweep on Propeller Performance,"AIAA Paper 77-176, June 1977

[5] Egolf, T. A., Anderson, O. L., Edwards, D. E., and Landgrebe, A. J.," An Analysis for High Speed Propeller-Nacelle Aerodynamic Performance Prediction; Volume 1, Theory and Initial Application and Volume 2, User's Manual for the Computer Program," United Technologies Research Center, R79-912949-19, June 1979.

[6] Hanson, D. B.," Compressible Lifting Surface Theory for Propeller Performance Calculation," AIAA paper 82-0020.

[17] Kaza, K. R. V., et al.,"Analytical Flutter Investigation of a Composite Propfan Model," Journal of Aircraft, Vol. 26, No. 8, pp 772-780, August 1989.

[18] Subrahmanyan, K. B., Kaza, K. R. V., Brown, G. V., and Lawrence, C.," Nonlinear Bending-Torsional Vibration and Stability of Rotating, Pretwisted, Preconed Blades Including Coriolis Effects," NASA TM 87207, 1986.

[19] "The NASTRAN Theoretical Manual," NASA SP 221(06), 1981.

[20] August, R., and Kaza, K. R. V.," Vibration, Performance and Flutter Response Characteristics of a Large-Scale Propfan and its Aeroelastic Model," AIAA Paper 88-3155, 24th Joint Propulsion Conference, Boston, Massachusetts, July 11-13, 1988.

[21] Ruo, S. Y., and Sankar, L. N., "Euler Calculations for Wing-Alone Configuration," *Journal of Aircraft*, Vol. 25, No. 5, pp 436-441, May 1988.

[22] Wake, B. E., and Sankar, L. N., "Solutions of the Navier-Stokes Equations for the Flow about a Rotor Blade," *Journal of the American Helicopter Society*, Vol. 34, No. 2, pp 13-23, April 1989.

[23] Rohrbach, C., Metzger, F. B., Black, D. M., and Ladden, R. M., "Evaluation of Wind Tunnel Performance Testings of an Advanced 45° Swept Eight-Bladed Propeller at Mach Numbers From 0.45 to 0.85," NASA CR-3505, 1982.

[24] Sullivan, W. E., Turnberg, J. E., and Violette, J. A.," Large Scale Advanced Propfan (LAP) Blade Design," NASA CR 174790.

[25] Aiello, R. A., and Chi, S.," Advanced Composite Turboprops: Modeling, Structural and Dynamic Analyses," ASME Paper 87-GT-78, 1987.

[26] Chou, S., "SR7L Turboprop Blade Finite Element Model," Sverdrup Topical Report, March 1986.

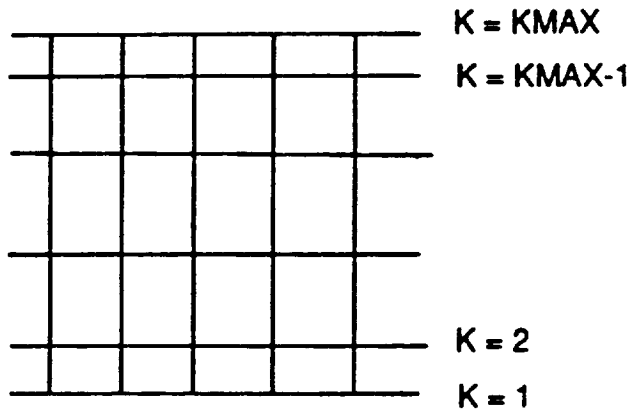

Figure-1a

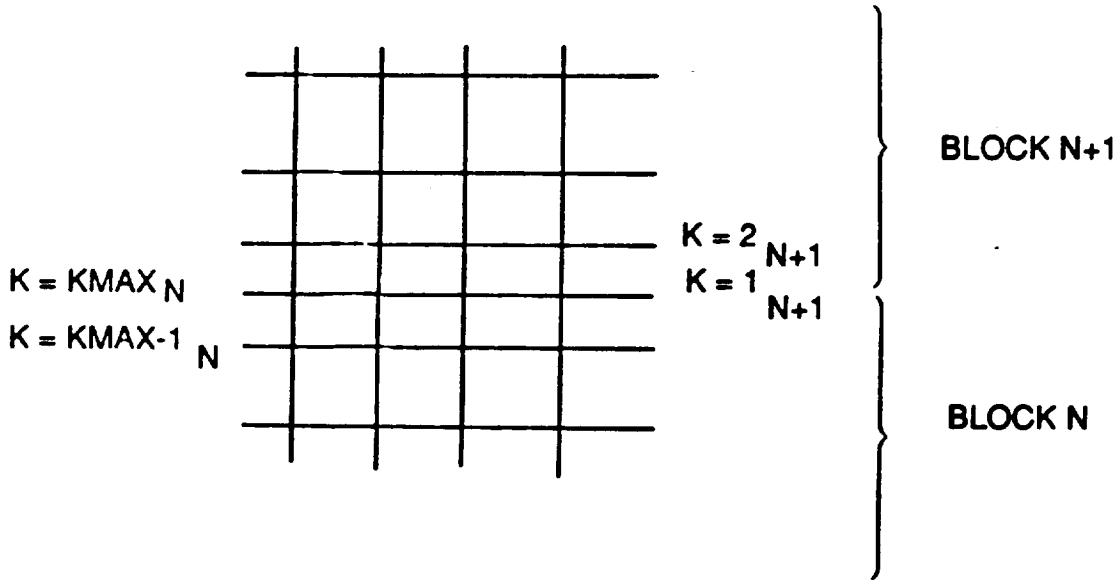

Figure-1b

Figure-1 Block-Interface Boundaries

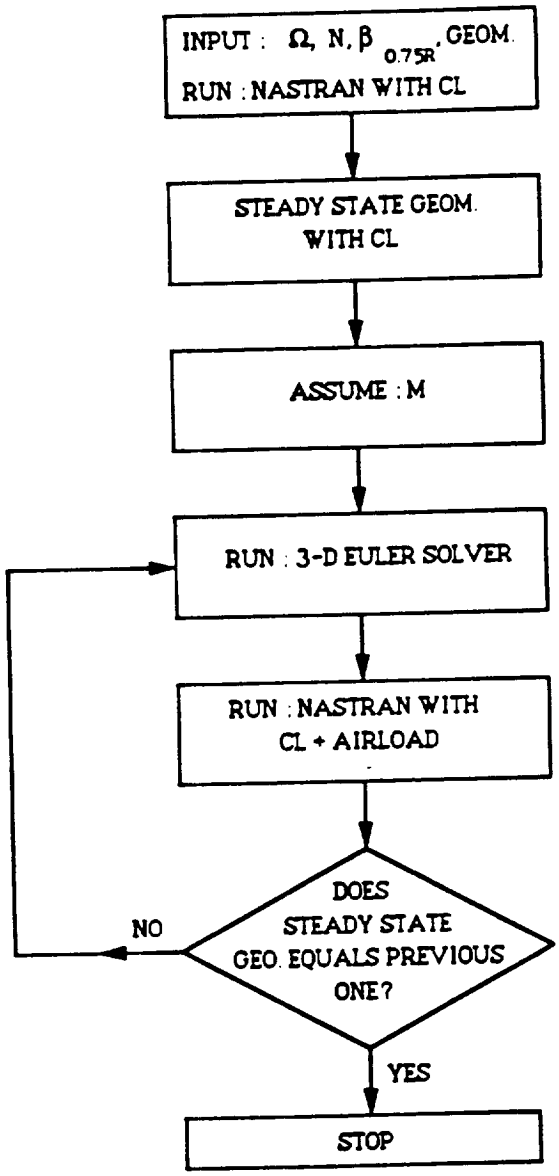

Figure-2 Flow Chart of the Aeroelastic Analysis

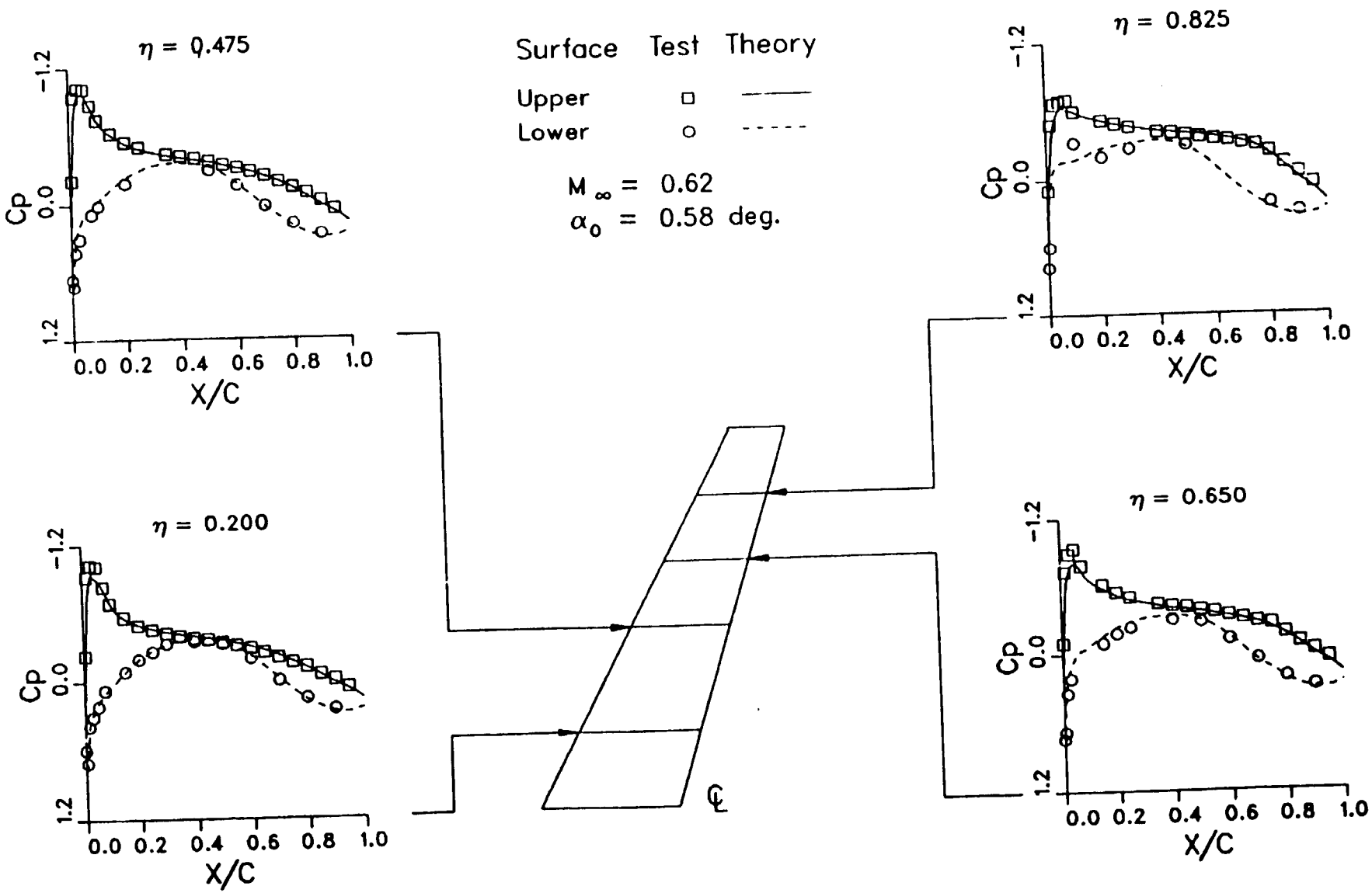

Figure-3 Euler Calculations for a Wing

Pressure Distribution

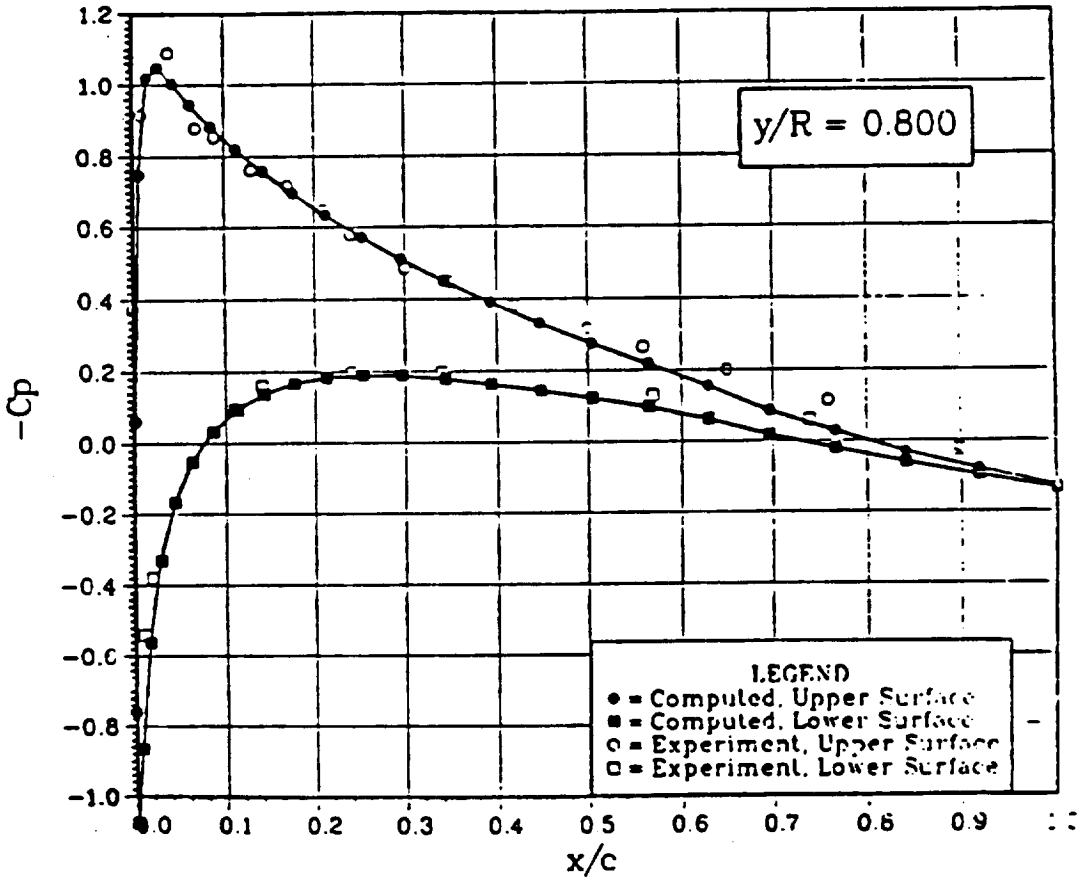

Figure-4a Pressure Coefficient for a NACA 0012 Rotor Blade in Hover

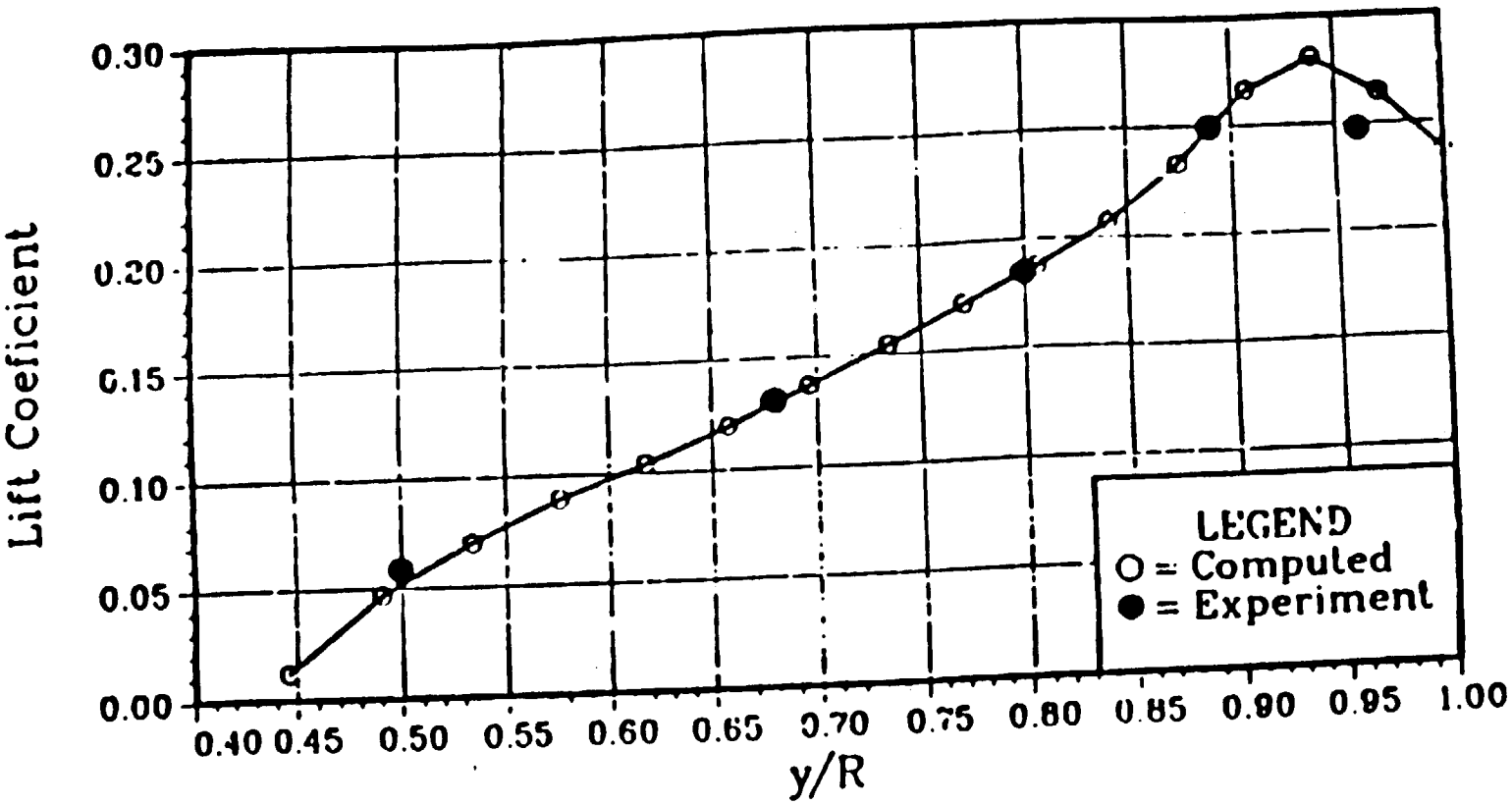

Figure-4b Lift Distribution for a NACA 0012 Rotor Blade in Hover

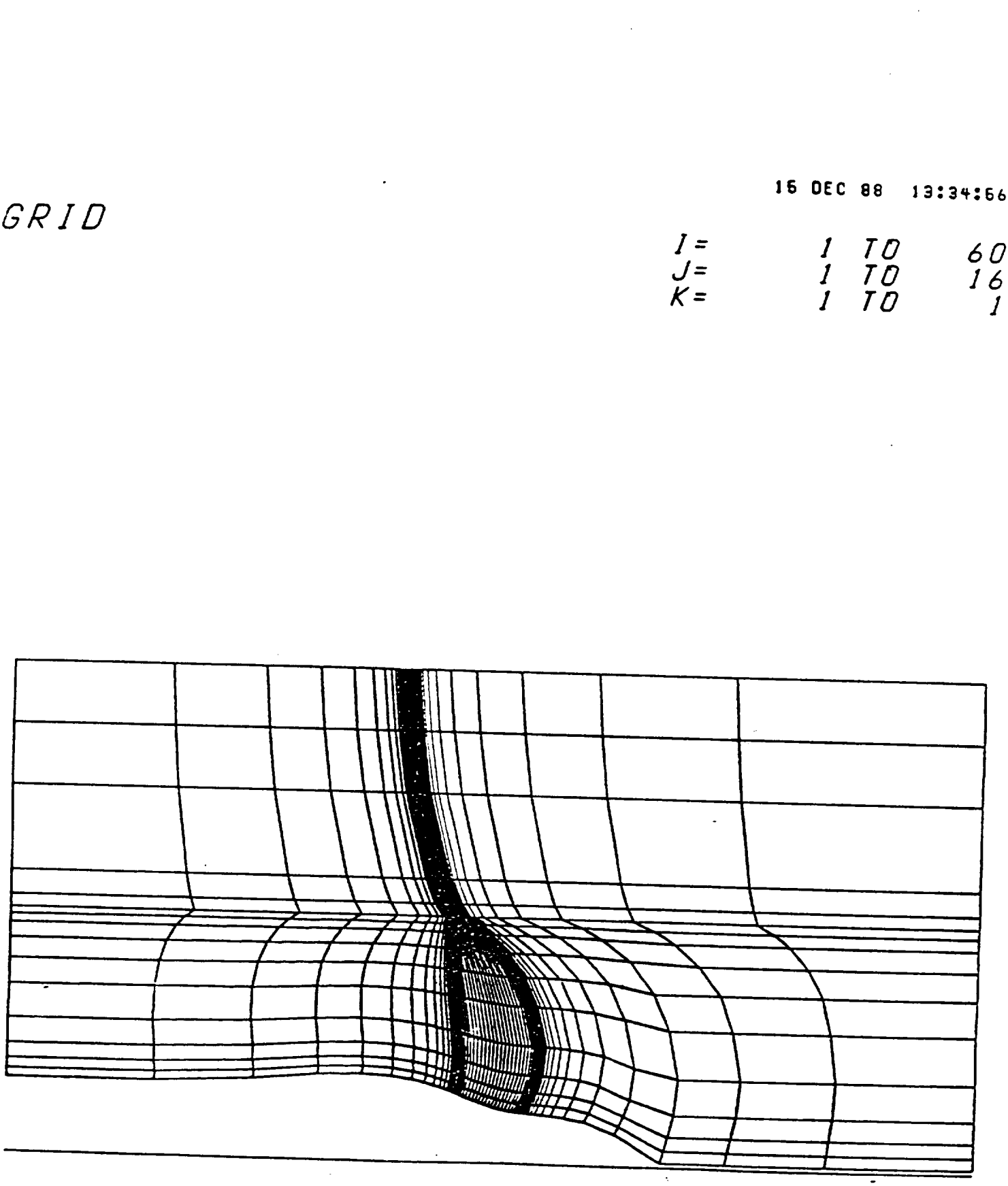

Figure-5a H-grid in Streamwise Plane

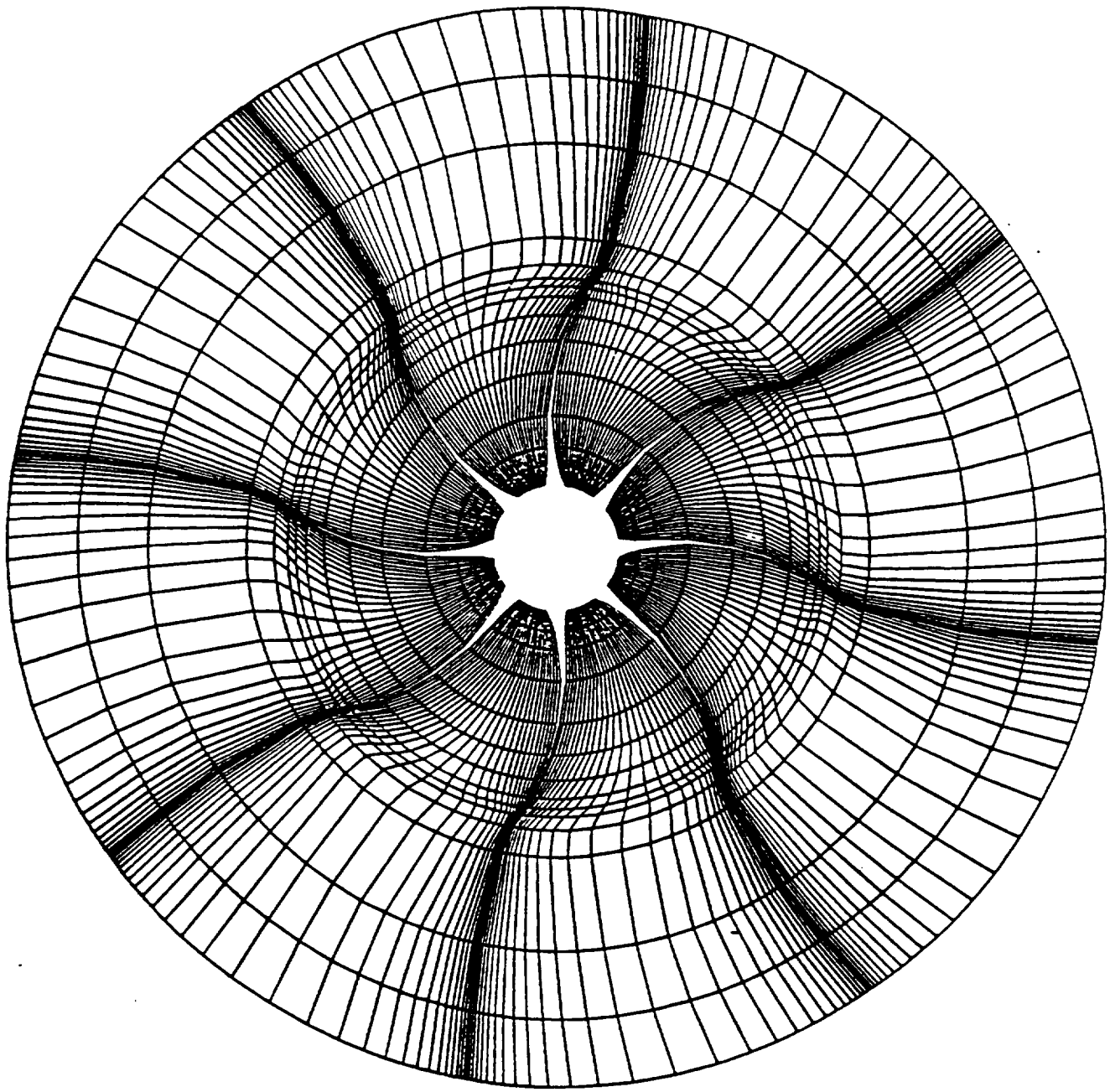

Figure-5b O-grid in Azimuthal Plane

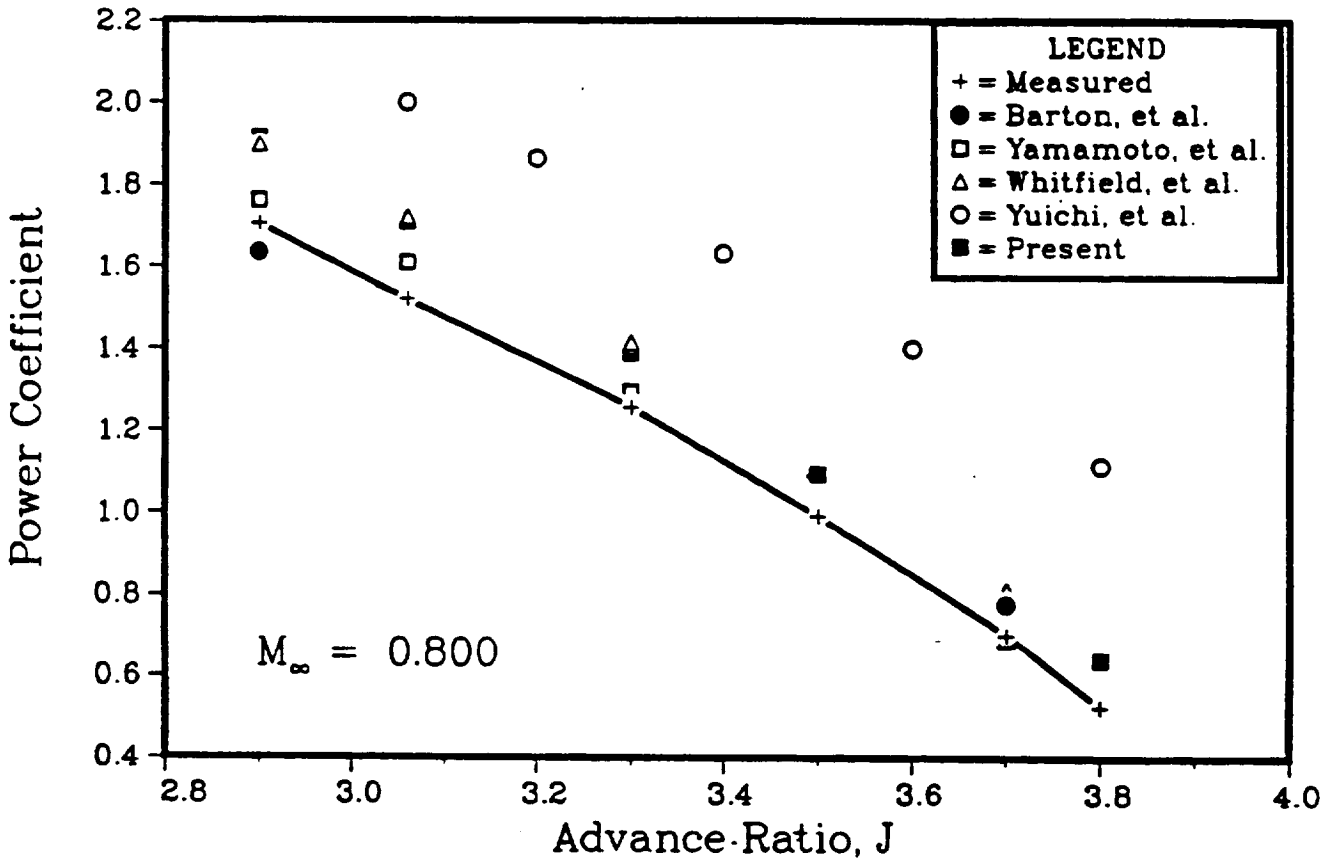
Power Coefficient vs. Advance Ratio
8 Bladed SR-3 Propfan
LEGEND
+ = Measured
● = Barton, et al.
□ = Yamamoto, et al.
△ = Whitfield, et al.
○ = Yuichi, et al.
■ = Present
M_∞ = 0.800
Power Coefficient
Advance-Ratio, J
2.2
2.0
1.8
1.6
1.4
1.2
1.0
0.8
0.6
0.4
2.8
3.0
3.2
3.4
3.6
3.8
4.0

Figure-6a

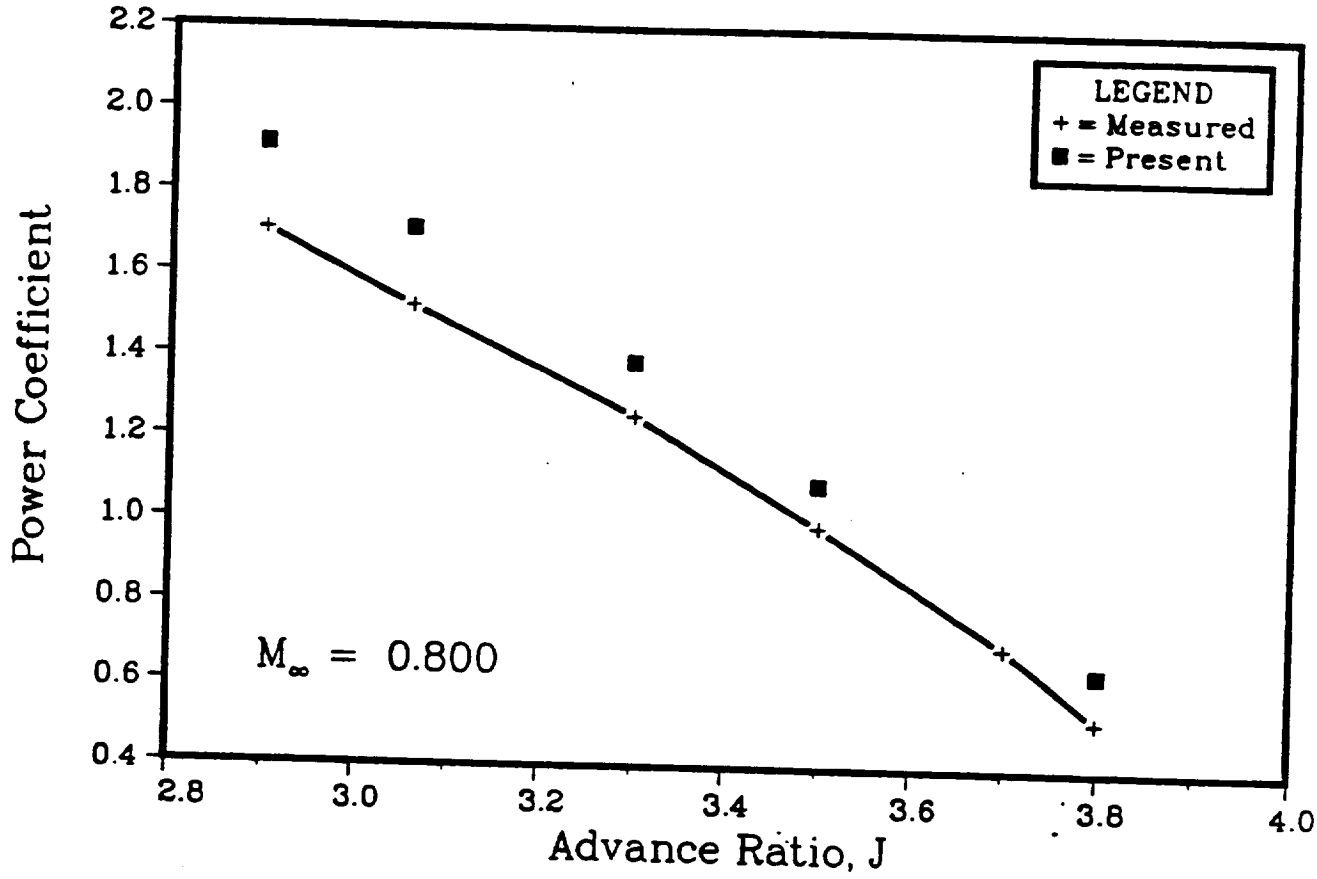
Power Coefficient vs. Advance Ratio
8-Bladed SR-3 Propfan
LEGEND
+ = Measured
■ = Present
M_∞ = 0.800
Power Coefficient
Advance Ratio, J
2.2
2.0
1.8
1.6
1.4
1.2
1.0
0.8
0.6
0.4
2.8
3.0
3.2
3.4
3.6
3.8
4.0

Figure-6b

SR-3 8-Bladed Propfan

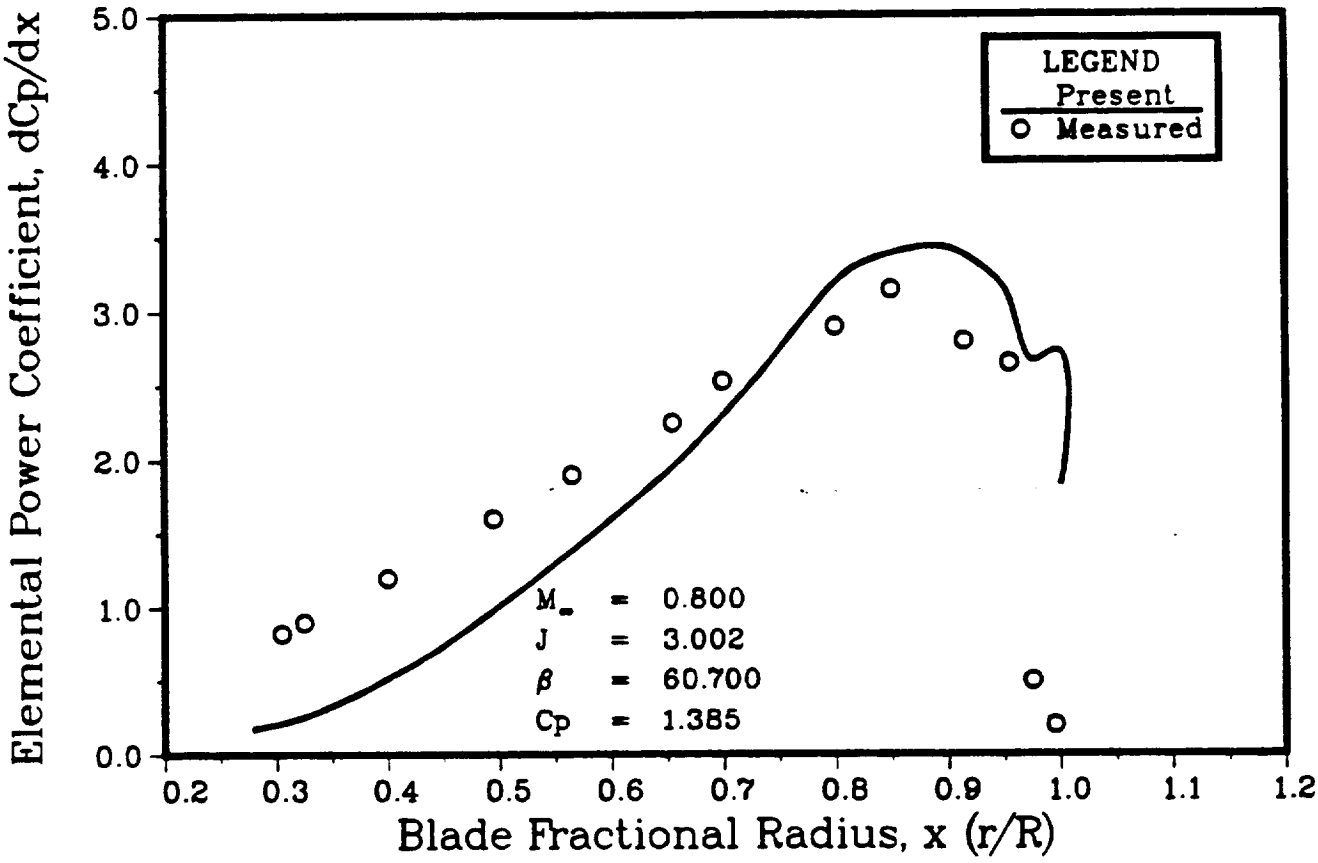

Figure-7

SR7L 2-Bladed Propfan

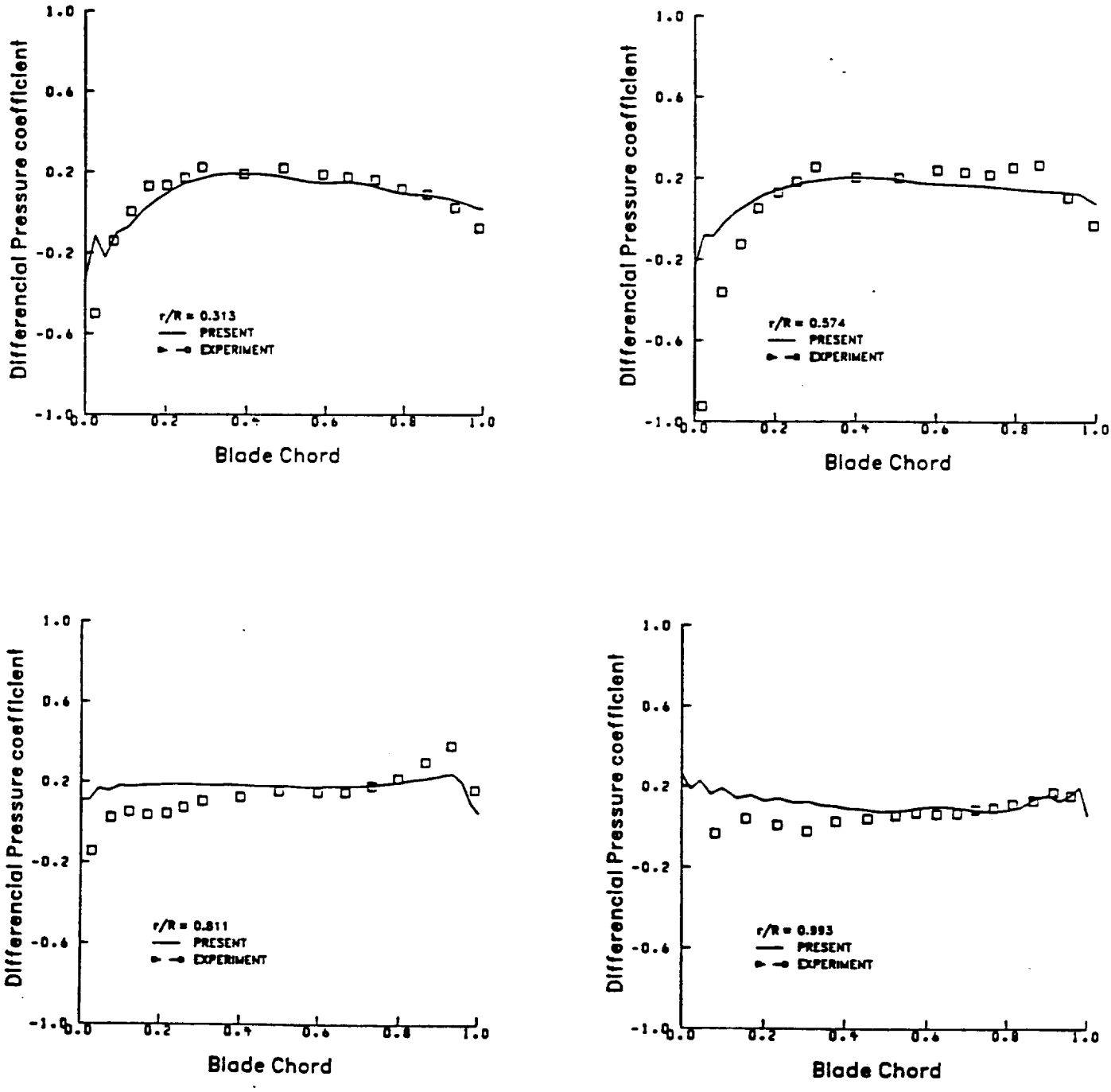

Figure-8 Differential Pressure Coefficient at Various Radial Locations $M_\infty = 0.775$, $J = 3.088$, $\beta = 54.6$

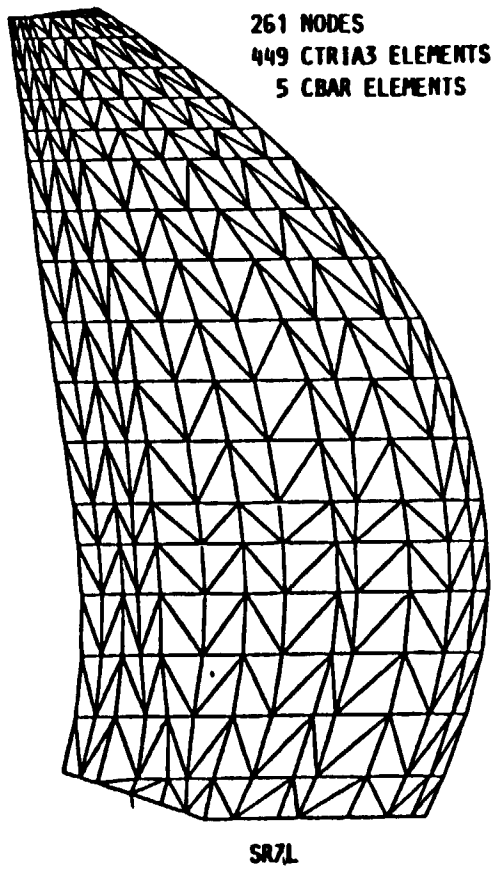

Figure-9a Propfan Blade Finite Element Model

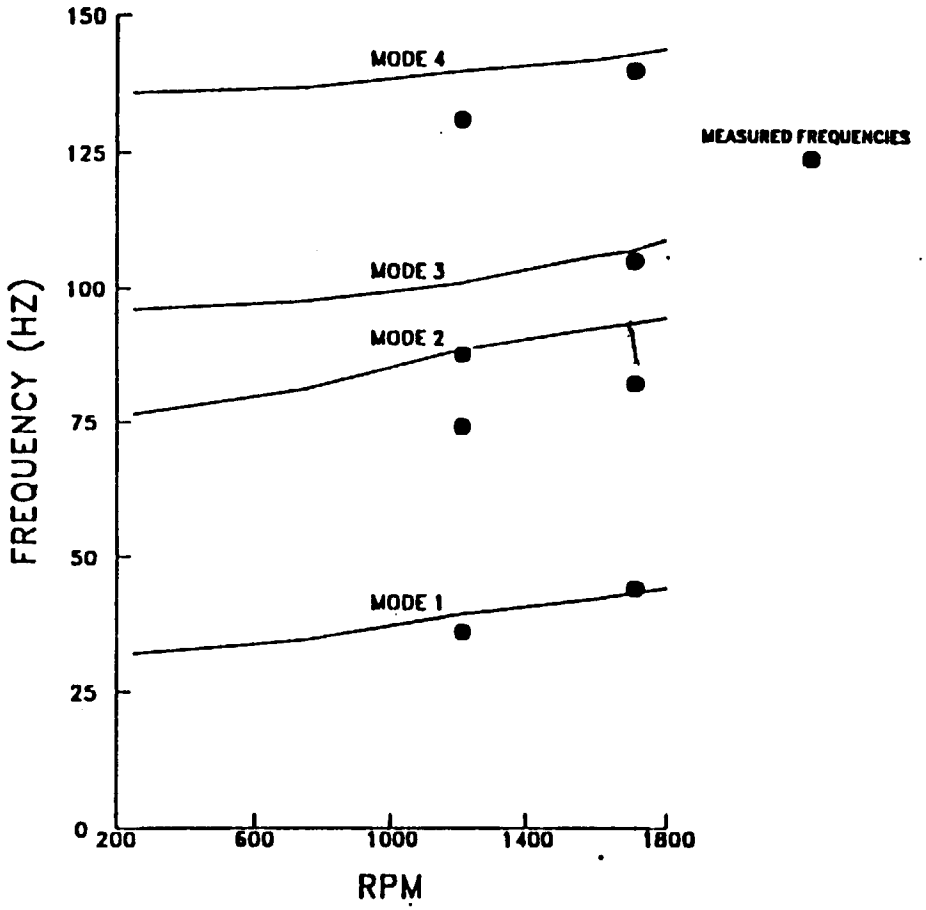

Figure-9b SR7L Frequencies - vs. - RPM

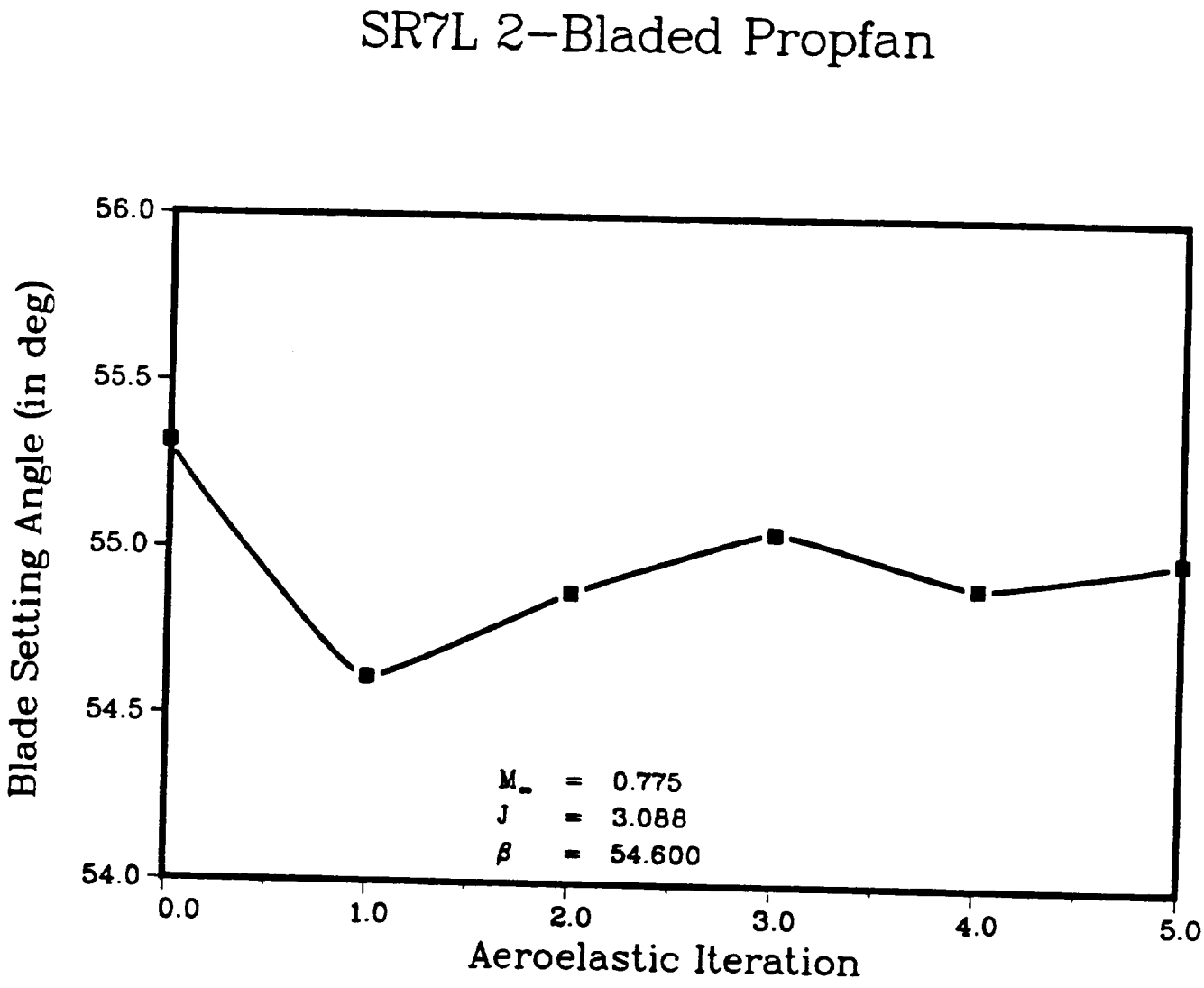

Figure-10 Blade Setting Angle at 75% Span versus Aeroelastic Iteration

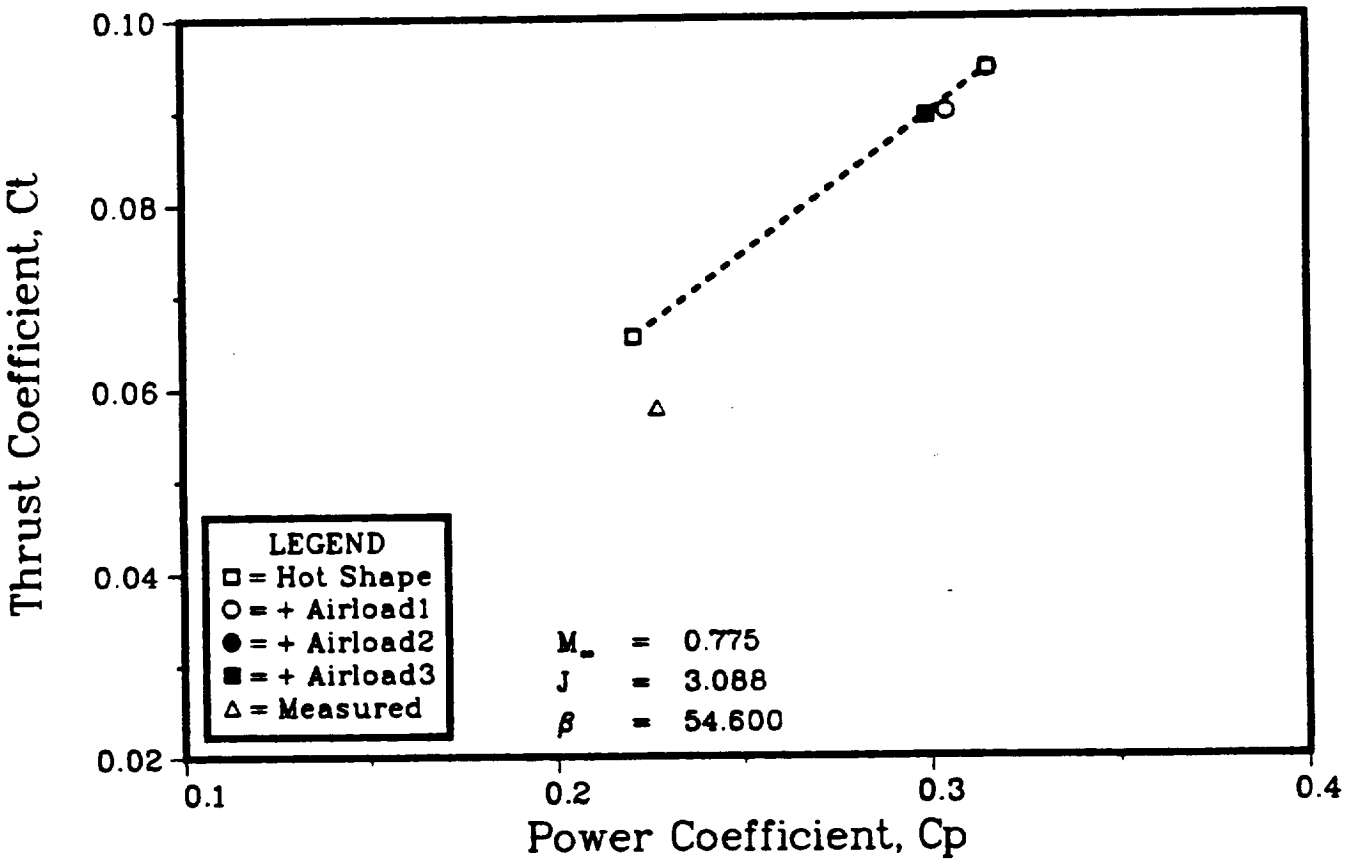

Figure-11 Calculated Thrust Coefficient versus Power Coefficient for Each Aeroelastic Iteration

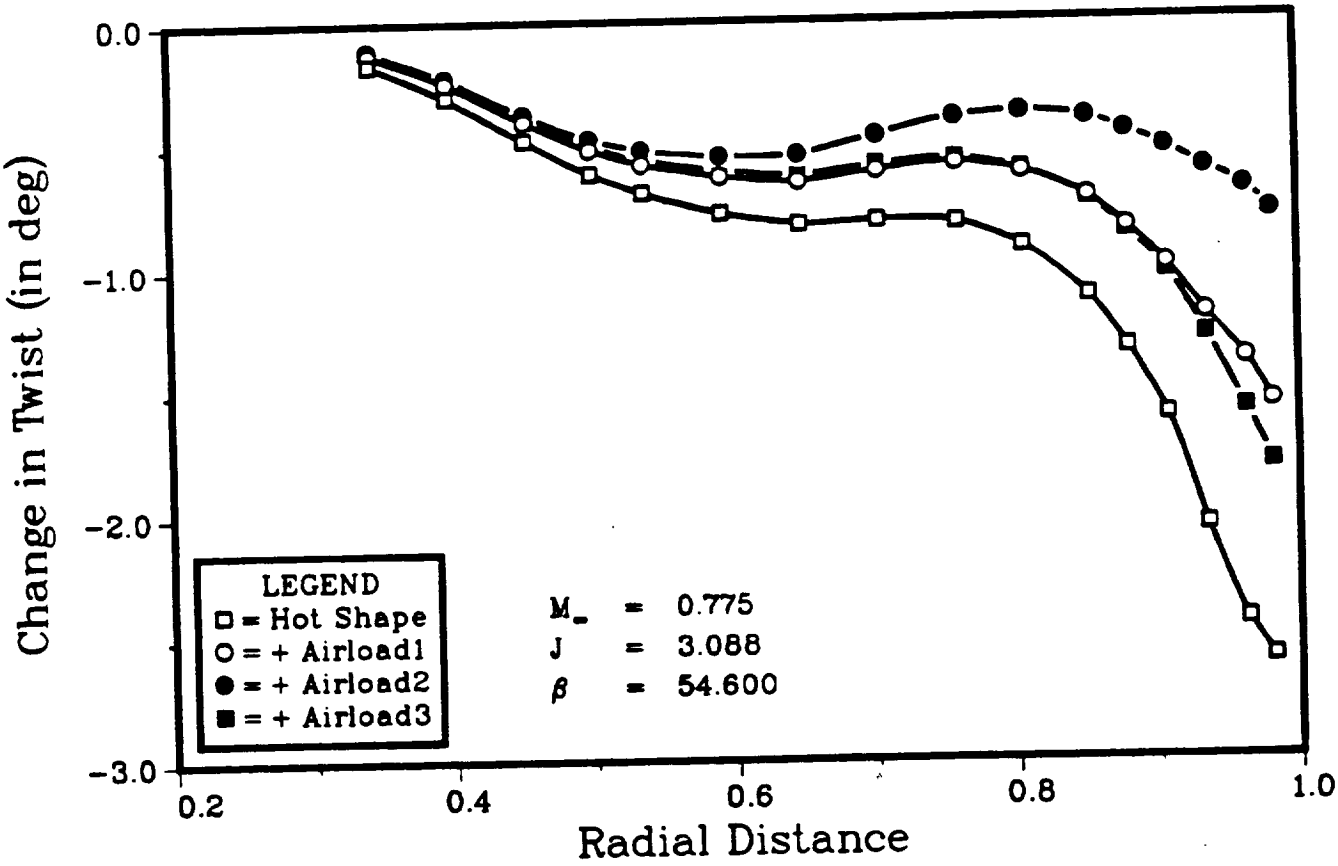

Figure-12 Change in Blade Setting Angle versus Blade Span
$M_\infty = 0.775$, $J = 3.088$

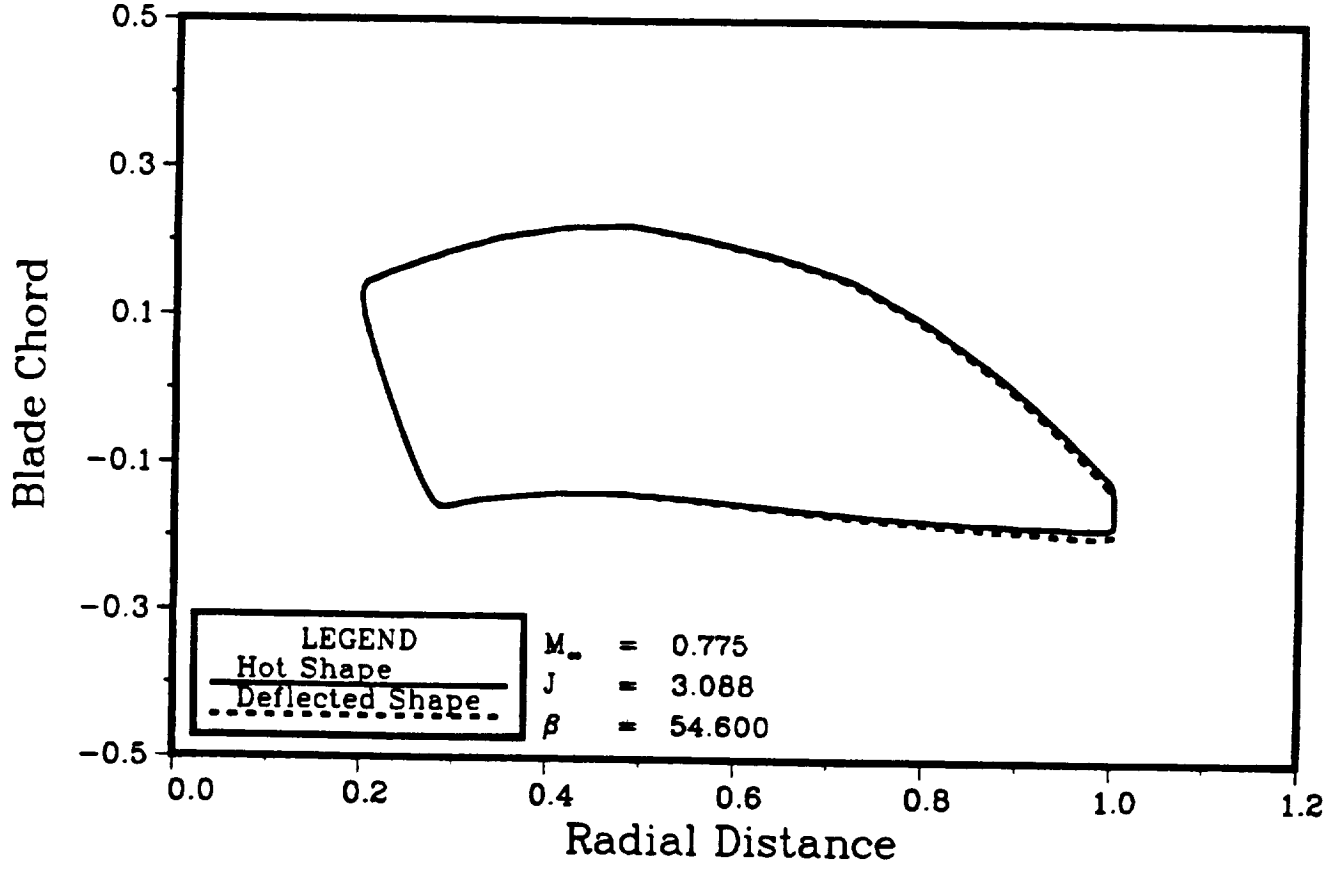

Figure-13 In Plane Deflection of Blade Planform
$M_\infty = 0.775$, $J = 3.088$, $\beta = 54.6$

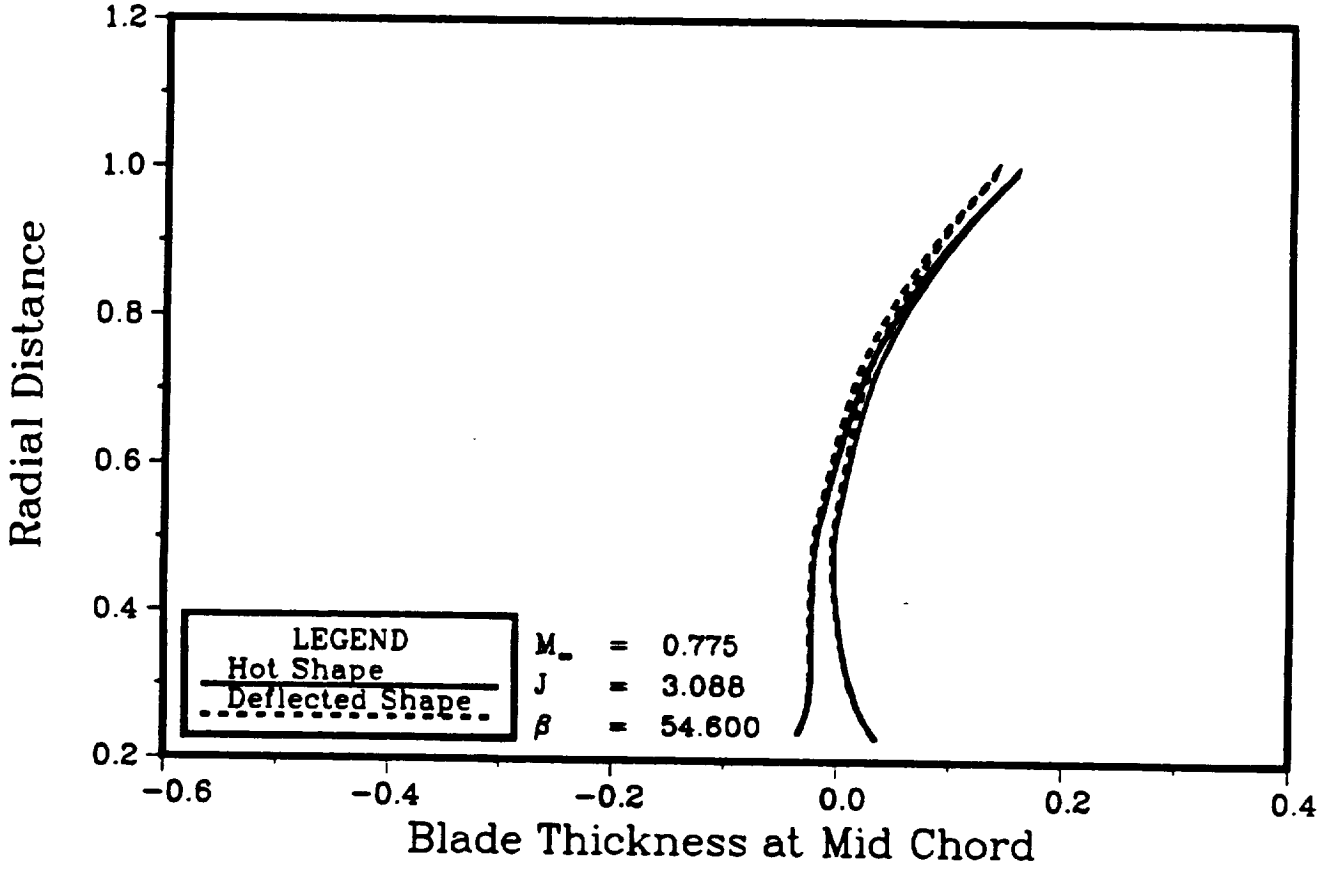

Figure-14 Out of Plane Deflection at Mid Chord
$M_\infty = 0.775$, $J = 3.088$, $\beta = 54.6$